

Realization of corner and helical edge states in topologically trivial band gap by twig edge

Jianfei Li,¹ Ying Wang,^{1,2,3} Zhongxiang Zhou,^{1,2,3} Jingfeng Yao,^{1,2,3,*} Zhihao Lan,^{4,†} and Chengxun Yuan^{1,2,3,‡}

¹*School of Physics, Harbin Institute of Technology, Harbin 150000, People's Republic of China*

²*Heilongjiang Provincial Key Laboratory of Plasma Physics and Application Technology, Harbin 150000, People's Republic of China*

³*Heilongjiang Provincial Innovation Research Center for Plasma Physics*

and Application Technology, Harbin 150001, People's Republic of China

⁴*Department of Electronic and Electrical Engineering, University College London, Torrington Place, London WC1E 7JE, United Kingdom*

The twig edge states in graphene-like structures are viewed as the fourth states complementary to their zigzag, bearded, and armchair counterparts. In this work, we study a rod-in-plasma system in honeycomb lattice with twig edges under external magnetic fields and lattice scaling and show that twig edge states can exist in different phases of the system, such as quantum Hall phase, quantum spin Hall phase and insulating phase. The twig edge states in the quantum Hall phase exhibit robust one-way transmission property immune to backscattering and thus provide a novel avenue for solving the plasma communication blackout problem. Moreover, we demonstrate that corner and edge states can exist within the trivial band gap of the insulating phase by modulating the on-site potential of the twig edges. Especially, helical edge states with the unique feature of pseudospin-momentum locking that could be excited by chiral sources are demonstrated at the twig edges within the trivial band gap. Our results show that many topological-like behaviors of electromagnetic waves are not necessarily tied to the exact topology of the systems and the twig edges and interface engineering can bring new opportunities for more flexible manipulation of electromagnetic waves.

Introduction.— Graphene-like systems feature localized states at the boundaries, which exhibit distinctive transport properties than bulk states. In general, flat band with zero energy occurs at the zigzag edge, which is attributed to the non-binding orbital in the nearest neighbor tight-binding approximation [1, 2]. The bearded edge possesses a flat energy band complementary to the zigzag state, and the Tamm-like mode has been observed near the Van Hove singularity [3, 4]. However, there is no edge state for armchair boundary unless defects exist or lattice symmetry breaking occurs [1, 5–7]. As a magnetic field is applied to a graphene-like system, gapless edge states can be constructed on armchair boundaries, and a series of dispersionless bands emerge corresponding to the Landau levels [8]. Recently, a completely new boundary named “twig” has been proposed to realize the localization of light [9]. The twig edge along with the three boundaries mentioned above constitute the four basic boundary types in graphene structures. The substantial developments in topological physics in recent years have facilitated the interest in edge states. It is shown that robust edge states arise from the topological nature of the bulk Hamiltonian, which is summarized as the bulk-edge correspondence [10, 11]. When the time-reversal (TR) symmetry is preserved, a well known Wu-Hu model is proposed to realize photonic helical edge states by constructing pseudospin 1/2 states [12]. This well simulates the quantum spin Hall (QSH) effect in electronic systems utilizing all-dielectric photonic crystals. After this elegant proposal, scaling or rotation of circular rings and elliptical cylinders is proposed to realize the QSH effect in photonic systems with C_6 sym-

metry [13–15]. Between two photonic crystals with different topological properties, unidirectional edge states could be excited at the interface by chiral sources. The tunable directionality and robust properties can be extended to fabricate optical circuits and large-area topological waveguides [16, 17].

A recent study in [18] shows that none of the shrunken and expanded graphene-like lattices are topologically nontrivial in the sense that both phases show trivial Wilson loop without winding and consequently, localized Wannier function could be constructed. Nevertheless, the expanded phase has a nontrivial second Stiefel-Whitney number $\omega_2 = 1$, corresponding to the obstructed atomic limit, where the Wannier functions are located away from the center of the unit cell. A method recapitulating the Wu-Hu model by changing the shape of the rods in the honeycomb lattice can lead to fragile topology, where though the Wilson loop eigenvalues of certain isolated bands exhibit nontrivial windings with opposite slopes similar to the Z_2 insulators, the windings can be destroyed by adding trivial bands. [19]. The above results reveal that unidirectional transmission of edge states is not a specific feature of topology, i.e., helical edge states are strongly related to interface engineering, and unconventional transmissions can emerge by modulating the on-site edge potential [20–23].

In this letter, we develop a rod-in-plasma system to investigate twig edge behaviors in honeycomb lattice by simultaneously breaking TR symmetry and pseudo-TR symmetry, which is different from the rod-in-air systems, where edge states exist at the interface between two structures with different topological properties, or below

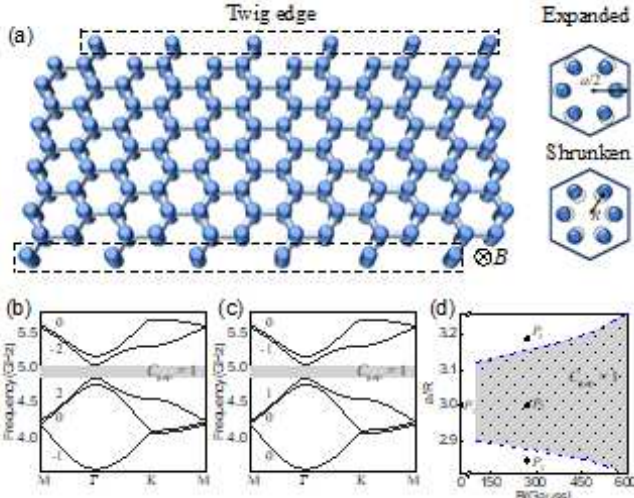


FIG. 1. The model of plasma photonic crystal with twig edges and the calculated band diagrams under expanded and shrunken cases. (a) PPC constructed by YIG rods immersed in plasma background with a magnetic field. The band diagram when the rods are (b) expanded by $R = a/2.95$ and (c) shrunken by $R = 3.05a$. Nontrivial band gaps with $C_{\text{gap}} = 1$ are obtained for both cases. (d) The phase diagram of PPC at different rod positions and magnetic fields.

the light cone without cladding structure [24, 25]. The plasma background originating from the communication blackout during the re-entry of the vehicle into the atmosphere provides a negative permittivity at a specific frequency [26, 27], which enforces an evanescent electromagnetic wave in plasma. This system elegantly emulates the electron behaviors described by tight-binding approximation [28, 29]. Under a magnetic field, the plasma photonic crystal (PPC) undergoes a phase transition from conventional insulator to Chern insulator and then to QSH insulator by changing the positions of the rods and the strength of the magnetic field. The tunable property has promising applications such as spin splitter device [30]. Our main finding is that, apart from the Chern insulator, novel twig edge states could exist in both trivial and nontrivial band gaps, where the bulk topology is not responsible for the nature of unidirectional transmission. Corner states can also be created in trivial band gaps, but without robustness. Importantly, terminating the system with a twig interface, helical edge states are successfully constructed in the trivial shrunken lattice, which has been verified to have a zero spin Chern number.

Plasma photonic crystal with twig edges.— We consider plasma photonic crystals as depicted in Fig. 1(a), where yttrium iron garnet (YIG) rods arranged in a honeycomb lattice are imbedded in plasma background and each unit cell contains six YIG rods (lattice constant $a = 40\text{mm}$, rod radius $r = 0.1a$, the distance between rod and center

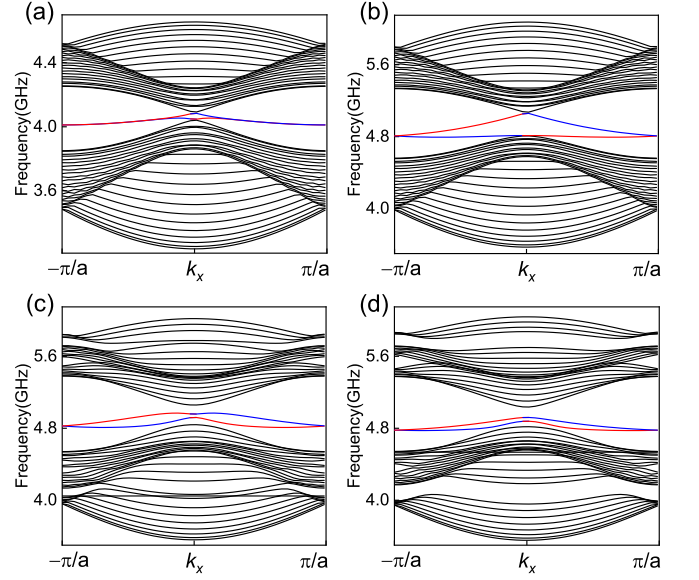


FIG. 2. The projected band diagram along the x direction for (a) P_1 , (b) P_2 , (c) P_3 , and (d) P_4 as marked in Fig. 1(d). The results show that gapless topological edge states exist in the nontrivial band gap, and the gapped edge states can be found both in expanded and shrunken cases.

of unit cell is R , electron density $n_e = 1 \times 10^{12}\text{cm}^{-3}$). The relative permittivity of plasma is $\varepsilon_r = 1 - \omega_{pe}^2/\omega^2$ (plasma frequency is expressed as $\omega_{pe} = ne^2/\varepsilon_0 m_e$, n represents the electron density, e the unit charge, ε_0 the permittivity in vacuum, and m_e the electron mass), where the collision frequency is neglected for simplicity. The plasma permittivity is negative when the incident wave frequency is lower than the plasma frequency. Permeability of the YIG rods could be expressed as a tensor when the external magnetic field is perpendicular to the structure, which leads to TR symmetry breaking of the system [31, 32]. The magnetized plasma has similar properties when the magnetic field is parallel to the structure, which can serve as a topological material [33–36]. The whole structure is terminated with twig-shaped edges that are viewed as the fourth type of edges of the honeycomb lattice[9].

We consider the case when the magnetic field is perpendicular to the structure and transverse magnetic (TM, E_z, H_x, H_y) modes of the electromagnetic wave will be considered in the following. The bands we focus on are below the plasma cutoff frequency, i.e., the YIG rods are surrounded by negative permittivity plasma. We first fix the magnetic field strength at 300 Gauss, and slightly expand ($R = a/2.95$) the six rods within a unit cell. The calculated band diagram is shown in Fig. 1(b), from which one can see an omnidirectional band gap between the third and fourth bands. As the TR symmetry of the system is broken, the bands could have different topological properties, which can be characterized by the Chen

number. The Chern number of each non-degenerate band is given by [2, 37, 38],

$$C_n = \frac{1}{2\pi} \iint_{BZ} \nabla_k \times A_{nk} d^2k \quad (1)$$

where A_{nk} is the Berry connection and can be expressed as

$$A_{nk} = -i \langle u_{nk} | \nabla_k | u_{nk} \rangle \quad (2)$$

with u_{nk} the spatially periodic part of the Bloch function of the n th band. By discretizing the Brillouin zone, the Chern numbers of the expanded lattice are calculated as -1, 0, 2, -2, 0 from the lower band to the upper band (see the marked Chern number for each band in Fig. 1(b)). The non-trivial nature of the bandgap is then evident by $C_{\text{gap}} = 1$. Next, we shrink the six rods within a unit cell by $R = 3.05a$, and the results are shown in Fig. 1(c). The shrunken case shares roughly the same band gap with Fig. 1(b), and the Chern number of the band gap is also $C_{\text{gap}} = 1$. Moreover, the topological properties of the bands can also be determined by their parities at the Γ point. The order of the eigenstates $[p_{\pm}, d_{\pm}]$ on either side of the band gap determines the QSH phase, the quantum Hall (QH) phase or the insulating phase of the system [30]. The phase diagram of the plasma photonic crystal under different magnetic fields and shrinking/expanding scales is obtained as shown in Fig. 1(d). The shaded area corresponds to the QH phase with $C_{\text{gap}} = 1$. As the six rods within the unit cell continue to shrink, the system transforms into an insulating phase. Below the shaded region of the phase diagram, the system is in the QSH phase. Next, we will choose four points in Fig. 1(d) (i.e., P_1, P_2, P_3 and P_4) to analyze the properties of the twig edge states.

The projected band diagrams of PPC for four situations.— To demonstrate the influence of twig edge on the non-bulk states, we select a supercell from Fig. 1(a) and calculate the band diagram projected in the x direction. In the absence of a magnetic field and lattice scaling, a full flat-band mode was found with nontrivial topological winding number [9]. Similar result can be observed for PPC as shown in Fig. 2(a), which corresponds to P_1 in Fig. 1(d). A nearly flat band appears across the Brillouin zone, and the lower twig edge state (red line) degenerates with the upper one (blue line). When the TR symmetry is broken as described at P_2 , the degenerate twig edge states undergo splitting. A gapless edge state appears on each twig interface, corroborating the bulk-edge correspondence. For the case of P_3 , there are gapped edge states in the pseudo gap, and a discrete band spectrum appears near $k_x = 0$ [see Fig. 2(c)]. Different from the topological gapless edge states in the QSH system [8, 30], the twig edge states are pushed into the band gap. It depends strongly on the on-site boundary potential of the twig edge [39], and the sizes of the rods at the

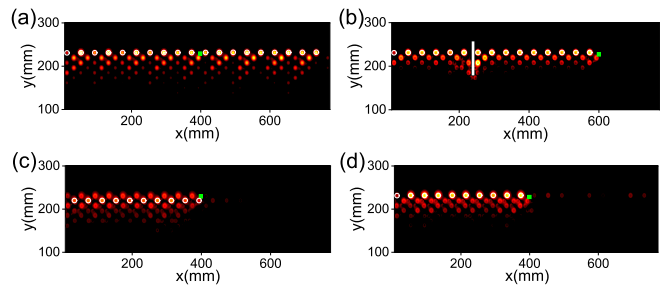


FIG. 3. Full-wave simulations of twig edge states excited by a line source for different cases: (a) magnetic field and lattice scaling are absent, which demonstrates the confinement of energy at the twig interface; (b) TR symmetry is broken, revealing the robustness of unidirectional transmission; (c) lattice expansion and magnetic fields are present, where mixed modes are demonstrated; (d) lattice contraction and magnetic fields are present, which exhibits a unidirectional propagation of twig edge states in a trivial band gap.

twig edge enable the edge states to couple to the upper or lower bulk bands. As for the shrunken case described by P_4 , twig edge states can still exist in the trivial band gap as shown in Fig. 2(d). However, the distinctive property here is the existence of unidirectional transmission, which is not related to the bulk topology.

We further perform full-wave simulations to verify the four twig edge modes. The YIG rods corresponding to the four situations are imbedded in plasma background, and a line source is placed at the twig interface. When the lattice scaling and magnetic field are absent for the case of P_1 , the energy is localized at the twig interface and penetrates slightly into the interior of the PPC as shown in Fig. 3 (a). As the TR symmetry is broken for P_2 , unidirectional transmission can be observed in Fig. 3 (b) at 4.87 GHz. Importantly, the twig edge state in this case is robust to impurities and free from backward scattering. By this way, we realize the robust transmission of electromagnetic waves in the negative permittivity background, which provides a new approach to communication in the plasma blackout. As for the expanded case at P_3 , the twig edge state excited at 4.93 GHz is shown in Fig. 3 (c). One can see a clear mixed mode here in that the energy is predominantly localized to the inner rods of the twig interface. Interestingly, the twig edge mode at P_4 can also be unidirectionally excited in the insulating phase at 4.84 GHz [Fig. 3(d)]. In the trivial band gap, this phenomenon depends strongly on the sharply asymmetric reflection effect [40], which accounts for the unidirectional waves in a trivial band gap, with a weak surface electric field.

The on-site potential of the boundary can dramatically affect the dispersion characteristics of the edge states [21], which could bring novel effects for the twig edges. To demonstrate this, we consider the shrunken case, where gapped edge states exist within the topologically trivial

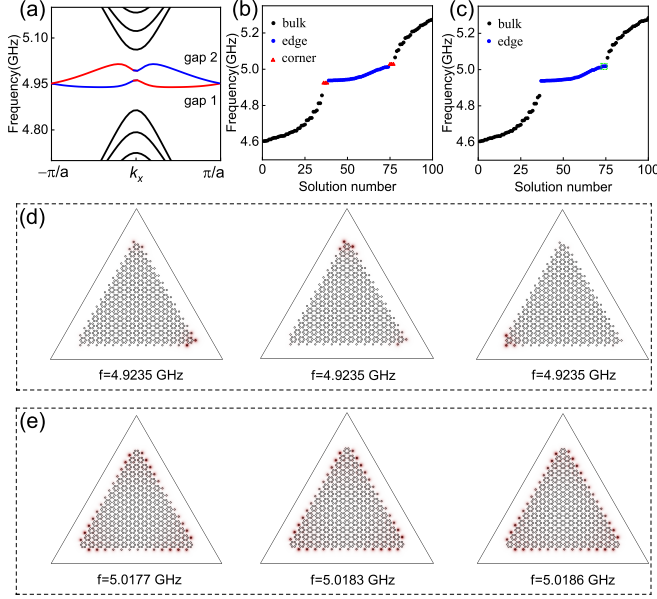


FIG. 4. Corner states in topologically trivial band gaps and modulated by twig interface. (a) The band diagram projected in the x direction for shrunken lattice with boundary atoms of size $0.092a$. By modulating the on-site boundary potential, the gapped edge states will be pushed into either the upper or lower bulk bands. (b) Calculated eigenmodes of a triangular-shaped supercell, where the black and blue dots represent the bulk and edge states respectively, whereas the red triangles denote the corner states. (c) The calculated eigenmodes when defects are present. (d) The field distributions (E_z) of corner states in gap 1. (e) The field distributions of edge states marked within the green box in Fig. 4(c).

band gap as shown in Fig. 2(d). As the size of the boundary atoms decreases, the edge states are gradually pushed into the upper bulk bands. On the other hand, the edge states will merge into the lower bulk bands when the size of the boundary atoms increases. The reason for this could be attributed to the fact that sufficiently small or large on-site potentials of the twig edges will lead to the decoupling of the twig edges from neighboring rods and as such, the system effectively terminates with armchair edges, where a complete band gap develops. When the size of the boundary atoms is fixed to $0.092a$, two band gaps named gap 1 and gap 2 appear near the edge states as shown in Fig. 4(a), within which corner states are expected. To show this, we construct a triangular-shaped supercell terminated with twig edges and containing 14-unit cells per edge, which is immersed into the plasma. The calculated eigenmodes of the supercell are shown in Fig. 4(b), from which one can see that corner states marked by red triangles exist in the two band gaps. The black and blue dots represent bulk and edge states respectively. For the corner states in gap 1, their electric fields (E_z) are localized at three different corners, respectively [see Fig. 4(d)] whereas the fields of corner states in gap

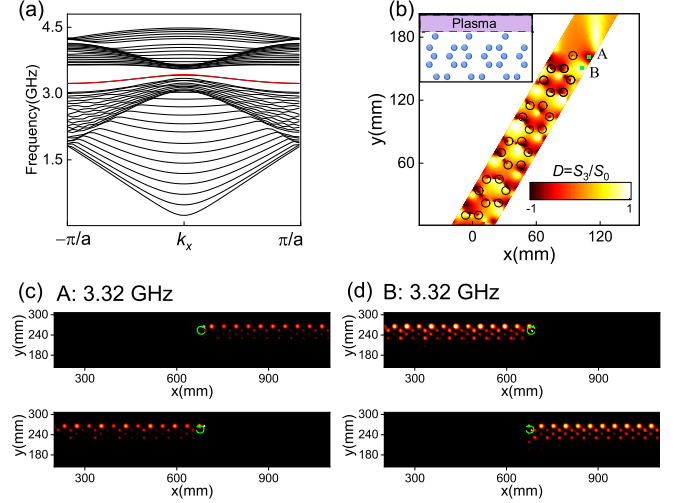


FIG. 5. Helical edge states at the twig edge of a shrunken lattice with trivial band gap. (a) The band diagram projected in the x direction, which shows a dispersive band of edge states in the topologically trivial band gap. (b) The schematic of the twig edge structure cladded by plasma, and the chirality map defined by the Stokes parameters S_0 and S_3 . Full-wave simulations of wave excited by the chiral source at the location marked by (c) A, and (d) B. The existence of modes with unidirectional propagation in the trivial band gap demonstrates that topology is not necessary for the helical edge states.

2 are distributed to three corners simultaneously (results not shown here). When small defects are introduced, e.g., one of the rods around the corner is removed, the spectrum differs remarkably as shown in Fig. 4(c), where the original corner states in gap 1 disappear, while the corner states in gap 2 are merged into the edge states. The field distributions of the merged edge states are shown in Fig. 4(e), from which one can see that the energy is mainly localized near the corners and then spreads towards the center of the edge. The results show that corner states can exist in topologically trivial band gaps due to twig edges, even though they do not share robust properties.

The realization of helical edge states in the shrunken case.— The invention of twig edge not only discovers a new localization mode [9], but also serves as a useful paradigm for interface engineering to explore the unconventional properties in topological physics. Here we consider a shrunken lattice with $R = a/3.15$ in the trivial regime, where the rods are placed into air without an external magnetic field, while the twig edge is enveloped in plasma [see the inset of Fig. 5 (b)]. The calculated projected band diagram is shown in Fig. 5(a). One can see that a dispersive band of edge states appears in the band gap due to the twig interface, which is not observed in structures with armchair edges. The twig edge can be treated as the type of defect when the honeycomb lattice is cut through the $1a$ Wyckoff position [18]. The local chirality of twig edge state can be

characterized as $D = S_3/S_0$ in terms of the Stokes parameter of the magnetic field, where $S_0 = |H_x|^2 + |H_y|^2$ and $S_3 = -2\text{Im}(H_x H_y^*)$ [41]. The chirality map of the edge state at $k_x = 0.48\pi/a$ is shown in Fig. 5(b), from which we can find distinct negative and positive chirality near the twig edge. As the chiral source is placed at the dark-red (point A) or bright yellow (point B) region, the directionality of electromagnetic waves may exhibit dissimilar property. Full-wave simulations for exploring the transmission properties are presented in Figs. 5(c) and (d). The chiral source constructed by four dipoles with clockwise or counterclockwise phases is placed at the negative chirality region marked by A. When the frequency is fixed at 3.32 GHz with clockwise phases for the chiral source, the mode with unidirectional propagation to the right is excited. As for the counterclockwise counterpart, the electromagnetic wave propagates unidirectionally to the left along the interface as shown in Fig. 5(c). The behavior will be reversed when the chiral source is placed at B, i.e., wave unidirectionally propagating to the left will be excited by the chiral source with clockwise phases and vice versa [see Fig. 5(d)]. By simply modulating the phase or position of the chiral source, the propagation direction of the electromagnetic wave can be efficiently manipulated. Thus, we realize the helical edge state without the requirement of topology, which reveals that spin-momentum locking is not a phenomenon necessarily tied to topology.

Conclusion.— We have developed the rod-in-plasma system, and studied the novel twig edge states under external magnetic field and lattice scaling. When the TR symmetry is broken, topological edge states exist at the twig interface, which can be maintained in limited shrunken and expanded lattices. The demonstration of robust transmission of electromagnetic waves in a negative permittivity background paves the way for solving the communication blackout problem in plasma. We have demonstrated that twig edge states can exist both in the QSH and trivial insulating phase. In the trivial band gap, corner states can be constructed when terminating the system with twig edges, which though are vulnerable to destruction by defects. In system preserving the TR symmetry, helical edge state excitable by chiral sources are formed in the topologically trivial band gap due to the twig interface. The new twig edge proves that topology is not necessary for helical edge states to exist. Our research provides new opportunities for the development of twig edge states.

Acknowledgments. This work was supported by the Natural Science Foundation of China (Nos. 12175050 and 12205067), and the Fundamental Research Funds for the Central Universities (Grant No. HIT. OCEF. 2022036).

* yaojf@hit.edu.cn

† lanzhihao7@gmail.com

‡ yuancx@hit.edu.cn

- [1] M. Kohmoto and Y. Hasegawa, Phys. Rev. B **76**, 205402 (2007).
- [2] T. Ochiai and M. Onoda, Phys. Rev. B **80**, 155103 (2009).
- [3] Y. Plotnik, M. C. Rechtsman, D. Song, M. Heinrich, J. M. Zeuner, S. Nolte, Y. Lumer, N. Malkova, J. Xu, A. Szameit, Z. Chen, and M. Segev, Nat. Mater. **13**, 57-62 (2014).
- [4] P. A. Pantaleón and Y. Xian, J. Phys. Soc. Jpn. **87**, 064005 (2018).
- [5] L.-Y. Zheng, F. Allein, V. Tournat, V. Gusev, and G. Theocharis, Phys. Rev. B **99**, 184113 (2019).
- [6] Z. Shi, M. Zuo, and H. Li, Results Phys. **24**, 104191 (2021).
- [7] Q. Tang, M. R. Belić, Y. Q. Zhang, Y. P. Zhang, and Y. D. Li, Nonlinear Dyn. **108**, 1573-1583 (2022).
- [8] J. L. Lado and J. F.-Rossier, arXiv:2210.07568.
- [9] S. Xia, Y. Liang, L. Tang, D. Song, J. Xu, and Z. Chen, Phys. Rev. Lett. **131**, 013804 (2023).
- [10] G. M. Graf and M. Porta, Commun. Math. Phys. **324**, 851-895 (2013).
- [11] M. Xiao, Z. Q. Zhang, and C. T. Chan, Phys. Rev. X **4**, 021017 (2014).
- [12] L.-H. Wu and X. Hu, Phys. Rev. Lett. **114**, 223901 (2015).
- [13] L. Xu, H.-X. Wang, Y.-D. Xu, H.-Y. Chen, and J.-H. Jiang, Opt. Express **24**, 18059-18071 (2016).
- [14] Z. Jiang, Y.-f. Gao, L. He, J.-p. Sun, H. Song, and Q. Wang, Phys. Chem. Chem. Phys. **21**, 11367-11375 (2019).
- [15] R. Zhou, H. Lin, Y. Liu, X. Shi, R. Tang, Y. Wu, and Z. Yu, Phys. Rev. A **104**, L031502 (2021).
- [16] M. Kim, Z. Jacob, and J. Rho, Light Sci. Appl. **9**, 130 (2020).
- [17] Z. Lan, M. L. N. Chen, J. W. You, and W. E. I. Sha, Phys. Rev. A **107**, L041501 (2023).
- [18] S. Xu, Y. Wang, and R. Agarwal, Phys. Rev. Lett. **131**, 053802 (2023).
- [19] M. Blanco de Paz, M. G. Vergniory, D. Bercioux, A. G.-Etxarri, and B. Bradlyn, Phys. Rev. Research **1**, 032005(R) (2019).
- [20] X.-D. Chen, F.-L. Shi, H. Liu, J.-C. Lu, W.-M. Deng, J.-Y. Dai, Q. Cheng, and J.-W. Dong, Phys. Rev. Applied **10**, 044002 (2018).
- [21] X. Xi, J. Ma, S. Wan, C.-H. Dong, and X. Sun, Sci. Adv. **7**, eabe1398 (2021).
- [22] M. Wang, Q. Ma, S. Liu, R.-Y. Zhang, L. Zhang, M. Ke, Z. Liu, and C. Chan, Nat. Commun. **13**, 5916 (2022).
- [23] G. Wei, Z. Liu, H. Wu, L. Wang, S. Wang, and J. Xiao, Opt. Lett. **47**, 3007-3010 (2022).
- [24] Y. Poo, R.-x. Wu, Z. Lin, Y. Yang, and C. T. Chan, Phys. Rev. Lett. **106**, 093903 (2011).
- [25] M. L. N. Chen, L. J. Jiang, Z. Lan, and W. E. I. Sha, Opt. Express **28**, 14428-14435 (2020).
- [26] J. P. Rybak and R. J. Churchill, IEEE Trans. Aerosp. Electron. Syst. **AES-7**, 879-894 (1971).
- [27] M. Keidar, M. Kim, and I. D. Boyd, J. Spacecr. Rockets **45**, 445 (2008).

- [28] J. Li, Y. Wang, Z. Zhou, J. Yao, J. Liu, Z. Lan, and C. Yuan, *Nanophotonics* **12**, 1847-1856 (2023).
- [29] J. Li, J. Yao, Y. Wang, Z. Zhou, A. A. Kudryavtsev, Z. Lan, and C. Yuan, *APL Photon.* **8**, 066102 (2023).
- [30] Z.-G. Chen, J. Mei, X.-C. Sun, X. Zhang, J. Zhao, and Y. Wu, *Phys. Rev. A* **95**, 043827 (2017).
- [31] Z. Wang, Y. D. Chong, J. D. Joannopoulos, and M. Soljačić, *Phys. Rev. Lett.* **100**, 013905 (2008).
- [32] Z. Wang, Y. D. Chong, J. D. Joannopoulos, and M. Soljačić, *Nature* **461**, 772-775 (2009).
- [33] W. Gao, B. Yang, M. Lawrence, F. Fang, B. Béri, and S. Zhang, *Nat. Commun.* **7**, 12435 (2016).
- [34] J. B. Parker, J. B. Marston, S. M. Tobias, and Z. Zhu, *Phys. Rev. Lett.* **124**, 195001 (2020).
- [35] Y. Fu and H. Qin, *Nat. Commun.* **12**, 3924 (2021).
- [36] N. Han, J. Liu, Y. Gao, K. Zhou, and S. Liu, *Phys. Rev. B* **105**, 235411 (2022).
- [37] C. Wang, H. Zhang, H. Yuan, J. Zhong, and C. Lu, *Front. Optoelectron.* **13**, 73-88 (2020).
- [38] R. Zhao, G.-D. Xie, M. L. N. Chen, Z. Lan, Z. Huang, and W. E. I. Sha, *Opt. Express* **28**, 4638-4649 (2020).
- [39] W. Yao, S. A. Yang, and Q. Niu, *Phys. Rev. Lett.* **102**, 096801 (2009).
- [40] S. Liu, W. Lu, Z. Lin, and S. T. Chui, *Phys. Rev. B* **84**, 045425 (2011).
- [41] Z. Lan, J. W. You, Q. Ren, W. E. I. Sha, and N. C. Panoiu, *Phys. Rev. A* **103**, L041502 (2021).